CrossMark

Investigation of effects of MgO nanoparticles addition on the superconducting properties of Bi-2223 superconductors

Tuğba Çördük[1] · Özlem Bilgili[1] · Kemal Kocabaş[1]

Abstract In this study, the effects of addition of magnesium oxide powders with average particle size <100 nm to Bi-2223 superconducting system were investigated. Bulk samples with general formula of $Bi_{1.7}Pb_{0.3}Sr_2Ca_2Cu_3O_y + (MgO)_x$ nominal composition (x = 0.00, 0.05, 0.10, 0.15 and 0.20 wt%) were prepared by conventional solid state reaction method. The critical temperature (T_c) and hole concentration (p) of nano MgO added samples were determined by AC susceptibility measurements. X-ray powder diffraction measurement (XRD) was used to examine phase formation, volume fraction and lattice parameters. The microstructure and surface morphology analyses of the samples were determined by scanning electron microscope. As Nano Mg addition was increased, surface morphology and grain connectivity of the samples were observed to degrade. XRD results showed that the lattice parameters do not change with increasing nano Mg addition. It was also observed from XRD measurements that volume fraction of Bi-2223 phase decreases with increasing nano Mg addition. The volume fraction of Bi-2223 phase for the non-added sample showed the highest value as 62.7% and further increasing nano MgO, the volume fraction of Bi-2223 phase decreases while Bi-2212 phase increases. The sample with 0.20 wt% MgO addition showed the highest volume fraction of Bi-2223 phase (~56%) and the highest superconducting transition temperature, T_c (~106 K) compared to added samples with nano MgO. The effect of nano Mg addition on magnetic properties of $Bi_{1.7}Pb_{0.3}Sr_2Ca_2Cu_3O_y$ superconductors were investigated by AC susceptibility measurements performed at ac fields of 1 Oe with f = 1000 Hz. The results revealed that critical temperature (T_c) decreases with increasing nano Mg addition down to 99.16 K.

1 Introduction

Since the discovery of high temperature superconductors (HTSCs), many studies have been done in Bi-2223 system in order to understand the structural, physical, and mechanical properties [1, 2]. Substitution or addition in the Bi-2223 system may lead to change in orientation of grains, oxygen amounts and crystal structures, which significantly affect J_c values of Bi-2223 ceramics [3]. Doping studies have demonstrated that substitution or addition of micro and nano-sized dopants is an efficient method to improve the inter-grain connectivity and flux pinning capability in Bi-2223 [4–6]. Recently, the effect of nano addition has been extensively studied to improve the superconducting properties such as nano elements (Ag, Au, etc.), nano oxides (SnO_2, ZrO_2, MgO, etc.) [7]. When nano particles are added to the Bi-2223 system, they can settle easier among the grains of these superconductors due to the small size of nanoparticles. Moreover, the addition of nano particles (10–60 nm) to the high-temperature superconductors plays an important role in enhancing the flux pinning and critical current density [8, 9]. On the other hand, substitution of nano particles significantly enhances the intergranular interaction. Nano-sized addition for Bi-2223 system, etc. MgO [10], Al_2O_3 [11], ZnO [12], Eu_2O_3 [13], SnO_2 [14], $NiFe_2O_4$ [15] and Fe_2O_3 [16] have been reported as showing improvement in the transport properties.

In many studies, the effects of nanosized particles addition on Bi-2223 system have been investigated.

✉ Özlem Bilgili
  ozlem.bilgili@deu.edu.tr

1 Department of Physics, Faculty of Science, Dokuz Eylül University, Izmir, Turkey

Yahya et al. [10] has reported the effects of different nanosized MgO on the transport critical current density of Bi-2223 phase. In their study, volume fraction was found to increas significantly with 20 nm MgO addition compared to pure sample and 40 nm MgO addition and high volume fraction were obtained for sample with x = 0.15 wt%. Suazlina et al. [17] reported the effects of Y_2O_3 nano particle addition in Bi-2212 superconductors. It was found that critical temperature and critical current density increased up to x = 0.7 wt%. Zelati et al. [18] have reported the effects of Dy_2O_3 nano particle addition on structural and superconducting properties of Bi-2223 system. According to their results, the best intergrain connectivity, the highest hole concentration and the best ac susceptibility measurements were obtained for sample with x = 0.5 wt% and T_c^{onset} was observed at 109.5 K. Zouaoui et al. [19] have studied effect of nano-size ZrO_2 addition on the flux pinning properties of (Bi–Pb)-2223 superconductor. Critical current density J_c behavior in applied magnetic field and volume pinning force density F_p are enhanced by the addition of 0.1 wt% ZrO_2, according to their study. Saad et al. [20] have studied the synthesized and characterization of Ag nano particles addition on Bi-2223 superconducting thin films. It was found that the highest volume fraction 66.15% of the Bi-2223 phase and the best critical temperature 103.5 K compared to other samples. As a result, T_c and volume fraction improved with increasing Ag nano particles to 1.0 wt%. Zelati et al. [13] reported the effects of Eu_2O_3 nano particles addition on structural and superconducting properties of Bi-2223 system. The results indicated that addition of Eu nano particle of the sample with x = 0.5 wt% improved the superconducting properties such as intergain connectivity and critical current density. These studies revealed that various nano particle addition increase the critical temperature (T_c) and intergrain connectivity which results in improvement of superconducting properties of Bi-2223 system.

With nanotechnology developments, a wide range of nanostructure materials have been synthesized [13]. In the nanosize range, the particles have a high proportion of atoms located at their surface as compared to bulk materials, giving rise to unique physical and chemical properties that are very different from their bulk counterparts [21]. Nanosized addition to Bi-2223 system has enhanced connectivity between the grains due to small sizes [13]. On the other hand, nanosized particles shed light the intergrain weak links in terms of intergranular critical current [22]. Furthermore, many efforts connected with adding or doping nano particles have been performed on the improvement of physical and magnetic properties of Bi-2223 system. It is obvious from these works that J_c values are positively affected when various nanosize particles such as

ZrO_2, SiC, MgO and Al_2O_3 into high temperature superconductors enter into BSCCO structure [22, 23].

In previous works, effects of superconducting parameters of nano-SnO_2 addition on Bi-2223 system and effect of Nb_2O_5 addition on superconducting properties of Bi-2223 system were reported [14, 24]. Additionally, Kocabas et al. [25] have investigated the effects of microsize Mg substitution in Bi-2223 superconductor and the highest critical temperature was reported as 112 K up to 0.10 content.

In this work, samples with different nano-MgO concentration (x = 0.00–0.20 wt%) were prepared using conventional solid state reaction method and the effects of nano-MgO particles on structural and superconducting properties of Bi-2223 based superconductor ceramics were investigated.

2 Experimental details

Superconducting samples with nominal composition $Bi_{1.7}Pb_{0.3}Sr_2Ca_2Cu_3O_y + (MgO)_x$ (x = 0.00, 0.05, 0.10, 0.15 and 0.20 wt%) were prepared by solid state reaction method, using Bi_2O_3, PbO, $SrCO_3$, $CaCO_3$ and CuO powders with high purity about 99.99% and nano-MgO. The samples were labeled as Mg0 (x = 0.00 wt%), Mg1 (x = 0.05 wt%), Mg2 (x = 0.10 wt%), Mg3 (x = 0.15 wt%) and Mg4 (x = 0.20 wt%), respectively. They were calcined at 800 °C for 15 h and then the powder mixture was again calcined at 820 °C for 15 h with intermediate grinding. The calcined samples were ground again and pressed into pellets 13 mm diameter and approximately 1.5-2 mm thick at 450–500 MPa pressure via a press machine. Finally, these pellets were sintered at 845 °C for 80 h and then cooled down to room temperature in air. The structure and phase of the samples were obtained by X-ray diffraction method (XRD) in 2θ = 3°–60° range with CuK$_\alpha$ radiation (λ = 0.15406 nm). Scanning electron microscopy (SEM) images were identified by using a SEM microscope. The ac susceptibility measurements were obtained using a homemade susceptometer and a lock-in amplifier (MODEL SR830 DSP Lock-in Amplifier). The density of the samples were calculated with the Archimedes method.

3 Results and discussion

Figure 1 shows X-ray diffraction patterns of all samples, where filled circle, open circle and filled diamond indicate the peaks due to Bi-(2223), Bi-(2212) and Ca_2PO_4 phases, respectively. XRD patterns of $Bi_{1.7}Pb_{0.3}Sr_2Ca_2Cu_3O_y + (MgO)_x$ (x = 0.00, 0.05, 0.10, 0.15 and 0.20 wt%) samples indicated that the majority of the peaks for all samples correspond to Bi-(2223), Bi-(2212) and the minority belongs to Ca_2PO_4 in
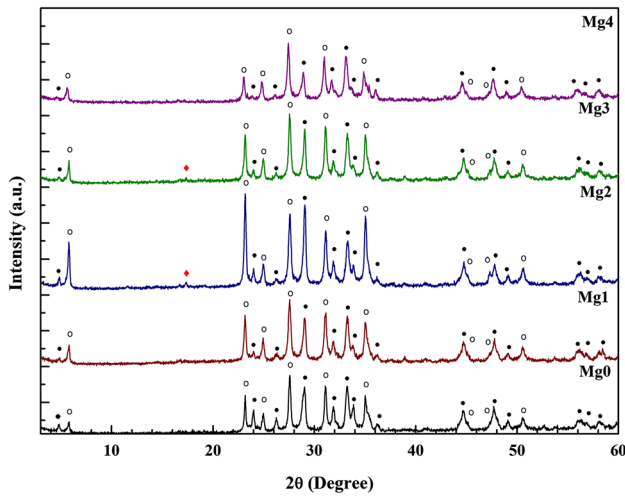
Fig. 1 XRD patterns of $Bi_{1.7}Pb_{0.3}Sr_2Ca_2Cu_3O_y + (MgO)_x$ samples (Mg0) x = 0.00, (Mg1) x = 0.05, (Mg2) x = 0.10, (Mg3) x = 0.15 and (Mg4) x = 0.20 wt%. Peaks of Bi-2223, Bi-2212 and Ca_2PO_4 phases are *filled circle*, *open circle* and *filled diamond*, respectively

samples Mg2 and Mg3 at 2θ = 17.88°. According to XRD measurements, the first peak which is important for Bi-2223 phase has been observed at 2θ = 4.7° whereas the second peak at 2θ = 5.7° corresponds to Bi-2212 phase. As seen 2θ = 4.7°, the first peak intensity decreases while the second peak intensity increases with nano-MgO addition. The most distinctive phases have been observed at 2θ = 23°–36°.

In order to determine the volume fraction of phases, all peak intensities of Bi-2223 and Bi-2212 phases and following formulas were used [26, 27];

$$Bi - (2223)\% = \frac{\sum I(2223)}{\sum I(2223) + I(2212)} \times 100$$

$$Bi - (2212)\% = \frac{\sum I(2212)}{\sum I(2223) + I(2212)} \times 100$$
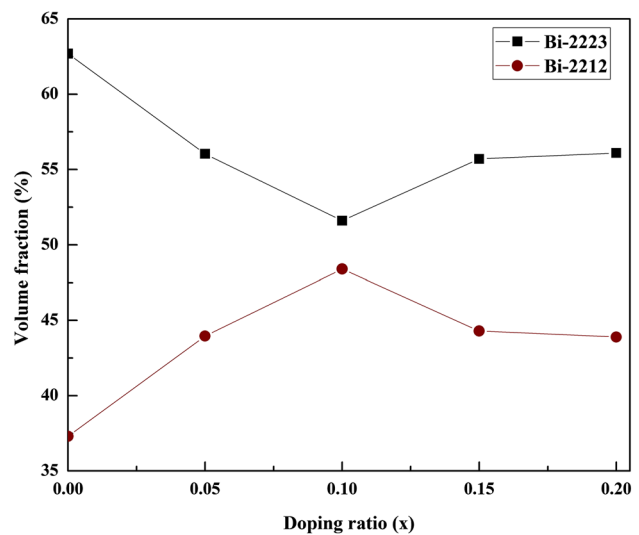
In equations, I(2212) and I(2223) are the intensities of XRD peaks for Bi-2212 and Bi-2223 phases, respectively [28]. The volume fractions of the phases for all samples are given in Table 1. As seen in the table, samples with x = 0.00, 0.05, 0.10, 0.15 and 0.20 wt% contained 62.70, 56.04, 51.60, 55.70% and 56.10 of the 2223 phase, respectively. It was observed that the percentage of 2223 phase decreases and the percentage of 2212 phase increases with increasing substitution of nano MgO (Fig. 2). Additionally, the intensity of the peaks corresponding to the Bi-2223 phase decreases and the intensities of peaks corresponding to Bi-2212 phase increase with further increase in nano MgO.

The values of grain size of all samples were calculated by using Scherrer Formula. Scherrer's formula;

$$L = \frac{0.9\lambda}{t\cos\theta}$$

L is the crystalline size in nm, λ is the wavelenght of X-ray in nm, t is the FWHM (full width at maximum) of the highest intensity peak and θ is the corresponding angle of the peak [29]. The grain sizes were calculated from XRD patterns and determined as 21.24, 21.40, 24.00, 24.82 and 21.30 nm for sample Mg0, Mg1, Mg2, Mg3 and Mg4, respectively. The results are presented in Table 1. According to table, the highest value of grain size was found as 24.82 nm for sample Mg3.

The lattice parameters a, b and c were calculated from Miller indices (hkl) and interplanar distances (d_{hkl}) by least squares method. The crystal system of non-added sample was found to be orthorhombic with the lattice parameters a = b = 5.406 Å and c = 37.120 Å. The nano

Table 1 The percentage volume fraction and grain size of Bi-2223 and Bi-2212 phases in $Bi_{1.7}Pb_{0.3}Sr_2Ca_2Cu_3O_y + (MgO)_x$ (x = 0.00–0.20 wt%) samples

Sample (wt%)	Volume fraction (±2) %		Grain size (±1) (nm)
	Bi-2223	Bi-2212	
0.00	62.70	37.30	21.24
0.05	56.04	43.96	21.40
0.10	51.60	48.40	24.00
0.15	55.70	44.30	24.82
0.20	56.10	43.90	21.30

Fig. 2 Volume fraction of Bi-2223 and Bi-2212 phases versus addition of nano MgO

Table 2 The lattice parameters (a, b and c) of Bi-2223 and Bi-2212 phases for samples Mg0, Mg1, Mg2, Mg3 and Mg4

Sample	Lattice parameters (Bi-2223 phase)			Lattice parameters (Bi-2212 phase)		
	a (Å)	b (Å)	c (Å)	a (Å)	b (Å)	c (Å)
Mg0	5.406	5.406	37.120	5.401	5.400	30.677
Mg0	5.399	5.413	37.130	5.394	5.398	30.638
Mg2	5.410	5.410	37.129	5.396	5.407	30.622
Mg3	5.399	5.413	37.130	5.398	5.400	30.649
Mg4	5.399	5.413	37.130	5.406	5.408	30.737

Table 3 The density values of all samples Mg0, Mg1, Mg2, Mg3 and Mg4

| Sample (wt%)	Density (±0.01) g/cm³
0.00	5.0370
0.05	5.1493
0.10	5.1237
0.15	5.1598
0.20	5.2308

MgO added samples showed almost no change in the lattice parameters. These results indicated that MgO does not enter $Bi_{1.7}Pb_{0.3}Sr_2Ca_2Cu_3O_y$ crystal structure and are given in Table 2.

The density of pellets were characterized according to the Archimedes principle in pure water and air. The density was calculated by using the formula;

$$\rho = \frac{W(h)[\rho(s) - \rho(h)]}{0.99983[W(s) - W(h)]} + \rho(h)$$

where $\rho(h)$ and $\rho(s)$ are in air and pure water densities and $W(h)$ and $W(s)$ are their weights. The densities of all samples are given in Table 3 and Fig. 3. The densities are 5.0370, 5.1493, 5.1237, 5.1598 and 5.2308 g/cm³ for samples Mg0, Mg1, Mg2, Mg3 and Mg4, respectively. The theoretical density of BPSCCO system is found as 6.3 g/cm³ from the lattice parameters [30, 31]. The density increased with increasing nano-MgO addition and the bulk densities obtained by Archimedes technique is in the range of 79.95–83.02% of the theoretical values. This result is in accordance with the porous structure (porosity) of ceramic superconductors. Porosity versus doping ratio graphic are given in Fig. 4.
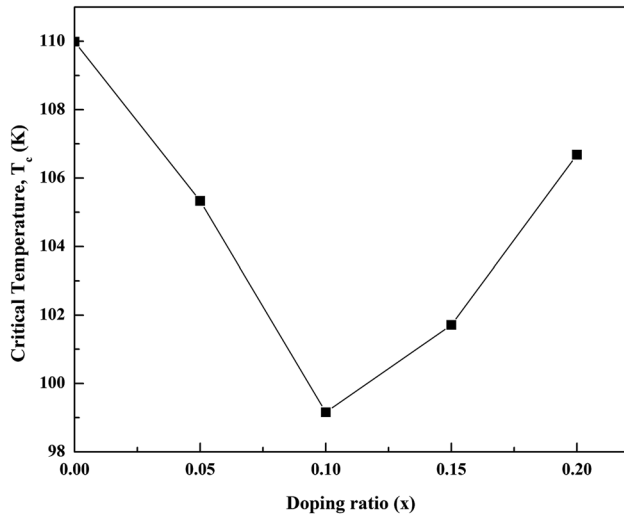
Critical temperature values were determined from AC magnetic susceptibility measurements. The variation of critical temperature T_c with Mg content is shown in Fig. 5. The measurements of susceptibility versus temperature for non-added and nano Mg-added samples have been plotted for AC field of 1 Oe with f = 1000 Hz. The critical transition temperatures (T_c) of Mg0, Mg1, Mg2, Mg3 and Mg4 samples are obtained to be about 109.99,
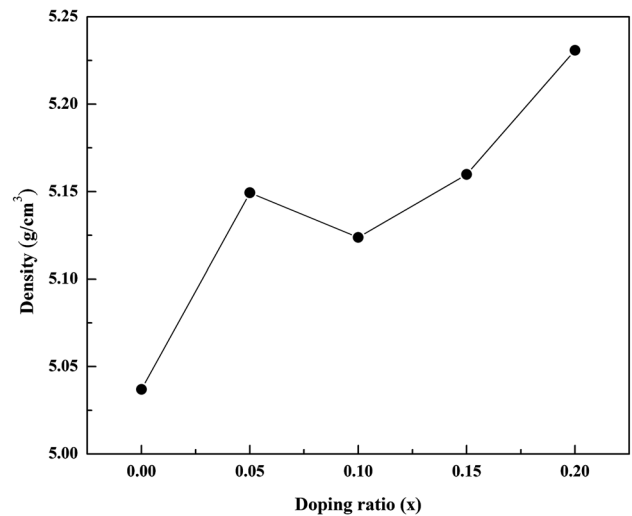
Fig. 3 Density of the samples versus doping ratio
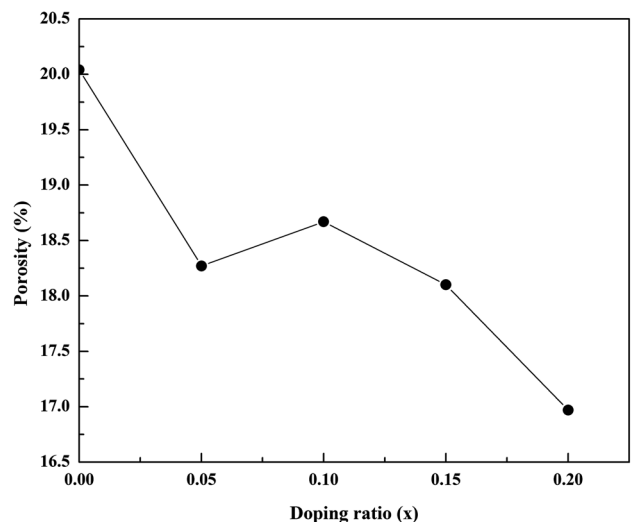
Fig. 4 Doping ratio versus porosity

105.33, 99.16, 101.71 and 106.68 K, respectively. The highest T_c (106.68 K) was observed at x = 0.20 wt% for nano MgO added samples. The non-added sample exhibited T_c of 109.99 K. Based on the results, the T_c value is found to decrease with the increase of the Mg addition
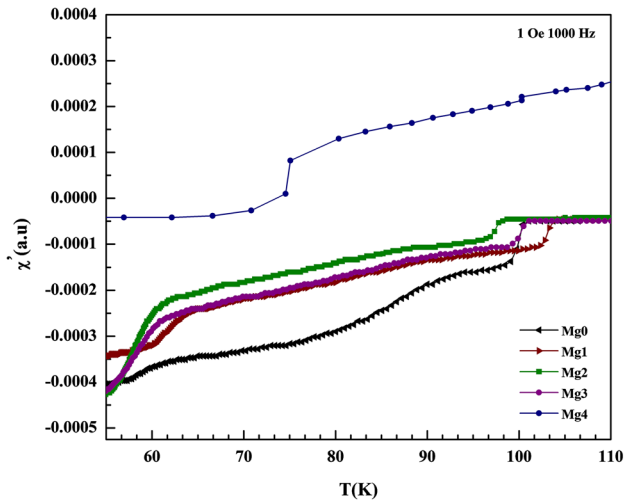
Fig. 5 The critical temperature versus (Mg0) x = 0.00, (Mg1) x = 0.05, (Mg2) x = 0.10, (Mg3) x = 0.15 and (Mg4) x = 0.20 wt%
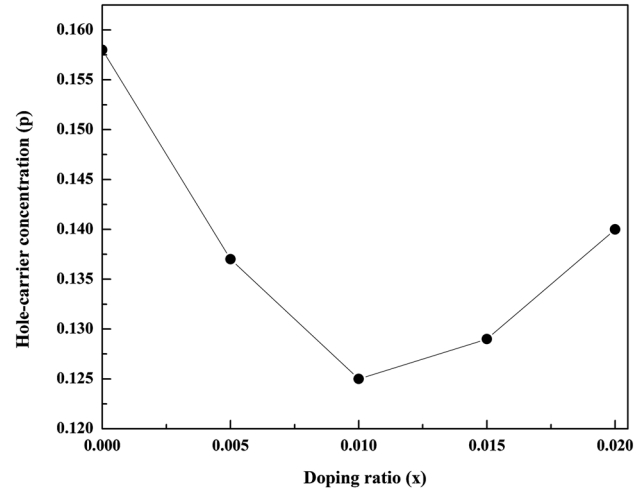
Table 4 Critical temperature and p (hole concentration) of the samples Mg0, Mg1, Mg2, Mg3 and Mg4

Sample (wt%)	T_c (±1) K	p (hole concentration)
Mg0	109.99	0.158
Mg0	105.33	0.137
Mg2	99.16	0.125
Mg3	101.71	0.129
Mg4	106.68	0.140

Fig. 7 The variation of hole concentrations versus nano-MgO content for the $Bi_{1.7}Pb_{0.3}Sr_2Ca_2Cu_3O_y + (MgO)_x$ samples (Mg0) x = 0.00, (Mg1) x = 0.05, (Mg2) x = 0.10, (Mg3) x = 0.15 and (Mg4) x = 0.20 wt%, respectively

Fig. 6 Variation of T_c critical temperature versus doping ratio for $Bi_{1.7}Pb_{0.3}Sr_2Ca_2Cu_3O_y + (MgO)_x$ samples (Mg0) x = 0.00, (Mg1) x = 0.05, (Mg2) x = 0.10, (Mg3) x = 0.15 and (Mg4) x = 0.20 wt%, respectively

(Fig. 6). This decrement is related to the increase of the relative percentage of 2212 phase formation.

Superconductivity occurs within the limits, $0.05 \leq p \leq 0.27$, which vary slightly in various cuprates [32]. Furthermore, the superconducting properties of Bi-2223 system are highly related to its hole concentration, pinning ability and its phase structure [33–35]. A parabolic relationship holds between the superconducting transition temperature and the hole concentration. The hole concentration is calculated using the relation given below:

$$p = 0.16 - [1 - T_c / T_c^{\max} / 82.6]^{1/2}$$

where $T_c^{\max}$ is taken as 110 K for (Bi–Pb)-2223 system [36, 37]. The hole concentration was observed as 0.158, 0.137, 0.125, 0.129 and 0.140 in samples Mg0, Mg1, Mg2, Mg3 and Mg4, respectively. The highest hole concentration is observed in sample Mg0 with x = 0.0% (Table 4).

Previous calculations for the unsubstituted Bi-2223 had shown that the values of p ranged from 0.116 to 0.160 [38]. As seen Fig. 7, the relationship between critical temperature and hole concentration is almost parabolic. The hole concentration decreased with increasing nano-MgO and then increased with increasing nano-MgO addition. It is well known that decreases in the hole concentration cause to degradations in the superconducting properties of the system [39–41].

The grain structure and surface morphology of the samples were obtained by Scanning Electron Microscopy (SEM). Figure 8a–e shows SEM micrographs for
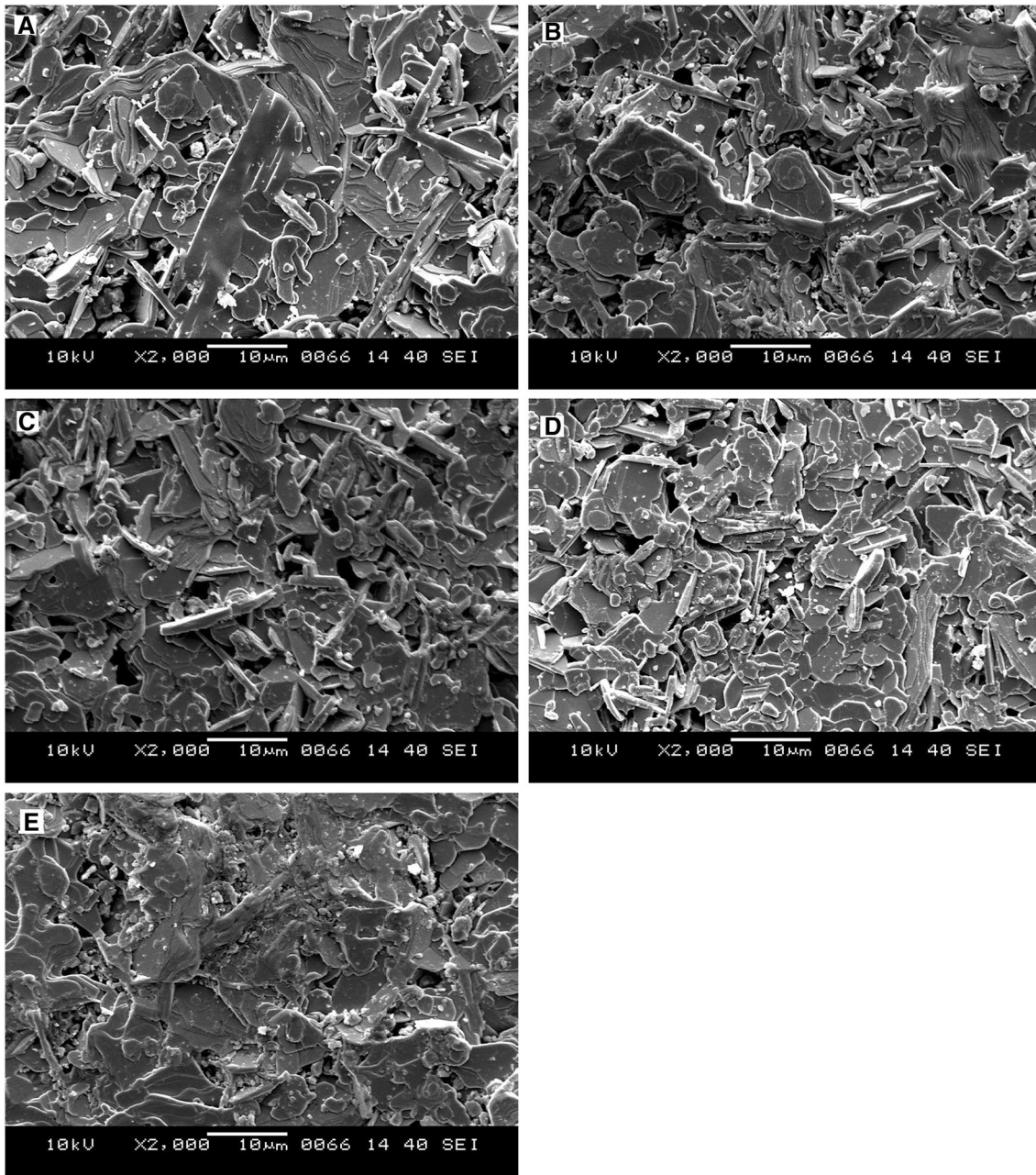
Fig. 8 SEM micrographs of Mg0, Mg1, Mg2, Mg3 and Mg4 samples

$Bi_{1.7}Pb_{0.3}Sr_2Ca_2Cu_3O_y(MgO)_x$ with x = 0.00, 0.05, 0.10, 0.15 and 0.20 wt%. It is observed that the microstructures of samples exhibit a common feature of plate-like grains. The grains are randomly distributed. The non-added sample consists of plate like grains as shown in Fig. 8a. Nano Mg added samples (Mg1–Mg4) contain small plate like grains while non-added sample (Mg0) consists of larger grains. Besides, the figure also shows some voids along the grain boundaries. Accordingly, it is seen that grains of the non-added sample are poorly connected. Microstructural

examination revealed that both the number and size of the voids decrease with increasing nano MgO substitution which may lead to increasing grain connectivity in the sample. In fact, this observation agrees with the experimentally measured density values of the same BSCCO samples (Table 3). It can be easily seen that while the non-added sample has the lowest density value, Mg4 sample has the highest density (or lowest porosity). The results of SEM measurements are consistent with XRD measurements. It is well known that grain alignment is related to the grain

connectivity. Larger grains with different orientation will clearly have larger misalignment and then lead to poor grain connectivity in microstructure. Additionally, the weak link effect of possible small voids may probably be higher at the grain boundaries with higher misalignment. Therefore, we may suggest that non-added sample has poorer grain connectivity due to large angle grain orientation mismatch as compared to other Mg added samples.

4 Conclusion

In this study, the samples with nominal composition $Bi_{1.7}Pb_{0.3}Sr_2Ca_2Cu_3O_y + (MgO)_x$ where x = 0.00, 0.05, 0.10, 0.15 and 0.20 wt% (<100 nm size) were prepared by solid state reaction method. The effects of nano MgO addition on the microstructue, phase formation, critical temperature of (Bi, Pb)-2223 were investigated by using XRD, SEM and ac susceptibility measurements.

The critical temperature was found as 109.99 K for the non-added sample and the sample with 0.20 wt% Mg addition had the highest T_c of 106.68 K among added samples. AC magnetic susceptibility measurements showed that hole concentration of the samples decrease with increasing MgO concentration. According to XRD measurements, non-added sample had the highest volume fraction of the Bi-2223 high-T_c phase (62.70%). Increasing the amount of nano Mg addition decreases the volume fraction of 2223 phase, while increasing volume fraction of 2212 phase. XRD shows that the addition of nano MgO does not change the crystallograpic structure of the samples and remained as orthorombic with the lattice parameters of a = b = 5.406 Å and c = 37.120 Å. Almost, the same lattice parameters were obtained for nano MgO added samples. SEM measurements showed that the plate like structure seems to be dominating the microstructure for all specimens. The surface morphology was seen to degrade and also the grain sizes of the samples are found to decrease with the increase of nano Mg addition. The addition of nano MgO increases the amount of random orientation plate-like grains and decreases its grain size. In our study, it was found that the addition of nano Mg has positive effect of decomposing the structure of high-T_c phase and enhancing low-T_c phase creation. Based on the above measurement results, it can be inferred that an non-appropriate amount of nano MgO may led to the degradation of the superconductivity of Bi-2223.

References

1. B. Ozkurt, M.A Madre, A. Sotelo, E. Yakinci, B. Ozcelik, J. Supercond. Nov. Magn. **25**, 799–804 (2012)
2. G. Yildirim, S. Bal, E. Yucel, M. Dogruer, M. Akdogan, A. Varilci, C. Terzioglu, J. Supercond. Nov. Magn. **25**, 381–390 (2012)
3. B. Ozkurt, J. Mater. Sci. **24**(11), 4233–4239 (2013)
4. A. Zelati, A. Amirabadizadeh, A. Kompany, H. Salamati, J.E. Sonier, J. Supercond. Nov. Magn. **27**, 2185–2193 (2014)
5. H. Sozeri, N. Ghazanfari, H. Ozkan, A. Kilic, Supercond. Sci. Technol. **20**, 522–528 (2007)
6. A. Ghattas, M. Annabi, M. Zouaoui, F. Ben Azzouz, M. Ben Salem, Phys. C **468**, 31–38 (2008)
7. A. Ishii, T. Hatano, Phys. C **340**, 173–177 (2000)
8. E. Guilmeau, B. Andrzejewski, J.G. Noudem, Phys. C **387**, 382 (2003)
9. H. Baqiah, S.A. Halim, M.I. Adam, S.K. Chen, S.S.H. Ravandi, M.A.M. Faisal, M.M. Kamarulzama M. Hanif, Solid State Sci. Technol. **17**, 81–88 (2009)
10. N.A.A. Yahya, R. Abd-Shukor, J. Supercond. Nov. Magn. **27**, 329–335 (2014)
11. A. Ghattas, F. Ben Azzouz, M. Annabi, M. Zouaoui, M. Ben Salem, J. Phys. **97**, 012175 (2008)
12. R. Mawassi, R. Awad, M. Roumie, M. Kork, I. Hassan, Adv. Mater. Res. **324**, 241 (2011)
13. A. Zelati, A. Amirabadizadeh, A. Kompany, H. Salamati, J. Sonier, J. Supercond. Nov. Magn. **27**, 1369–1379 (2014)
14. S. Yavuz, O. Bilgili, K. Kocabas, J. Mater. Sci. **27**, 4526–4533 (2016)
15. W. Kong, R. Abd-Shukor, J. Supercond. Nov. Magn. **23**, 257–263 (2010)
16. M. Roumié, S. Marhaba, R. Awad, M. Kork, I. Hassan, R. Mawassi, J. Supercond. Nov. Magn. **27**, 143–153 (2014)
17. M.A. Suazlinaa, S.Y.S. Yusaineea, H. Azhanb, R. Abd-Shukorc, R.M. Mustaqimd, Jurnal Teknologi **69**(2), 49–52 (2014)
18. A. Zelati, A. Amirabadizadeh, A. Kompany, H. Salamati, J. Sonier, Indian J. Sci. Technol. **7**, 123–134 (2014)
19. M. Zouaoui, A. Ghattas, M. Annabi, F. Ben Azzouz, M. Ben Salem, Supercond. Sci. Technol. **21**, 125005 (2008)
20. S.F. Oboudi, M.Q. Mustafa, Adv. Nanoparticles **5**, 75–82 (2016)
21. A. Zelati, Indian J. Sci. Technol. **6**, 5552–5558 (2013)
22. M. Annabi, A. M'chirgui, F. Ben Azzouz, M. Zouaoui, M. Ben Salem, Phys. C **405**, 25–33 (2004)
23. Z.Y. Jia, H. Tang, Z.Q. Yang, Y.T. Xing, Y.Z. Wang, G.W. Qiao, Phys. C **337**, 130–132 (2000)
24. O. Bilgili, K. Kocabas, J. Mater. Sci. **25**, 2889–2897 (2014)
25. K. Kocabas, O. Ozkan, O. Bilgili, Y. Kadıoglu, H. Yilmaz, J. Supercond. Nov. Magn. **23**, 1485–1492 (2010)
26. K. Kocabas, O. Bilgili, N Yasar, J. Supercond. Nov. Magn. **22**, 643–650 (2009)
27. S. Safran, A. Kılıc, E. Kılıcarslan, H. Ozturk, M. Alp, E. Asikuzun, O. Ozturk, J. Mater. Sci. **26**, 2622–2628 (2015)
28. M. Jafari, H. Sedghi, A. Esmaeili, J. Supercond. Nov. Magn. **26**, 3331–3338 (2013)
29. M. Anis-ur-Rehman, J. Alloys Compd. **469**, 66–72 (2009)
30. I.H. Gul, M. Anis-ur-Rehman, A. Maqsood, Phys. C **450**, 83–87 (2006)
31. X. Yang, T.K. Chaki, Supercond. Sci. Technol. **6**, 343–348 (1993)
32. F. Minghu, X. Zhuan, W. Hongbin, Z. Xingbin, H. Gangjin, Z. Xuanjia, C. Liezhao, Chin. Phys. Lett. **9**, 159–161. (1992)
33. O. Bilgili, K. Kocabas, J. Mater. Sci. **26**, 1700–1708 (2015)
34. R.P. Aloysius, P. Guruswamy, U. Syamaprasad, Supercond. Sci. Technol. **18**, L23–L28 (2005)
35. M. Maple, M. Brian, J Magn. Magn. Mater. **177**, 18–30 (1998)
36. V.G. Prabitha, A. Biju, R.A. Kumar, P.M. Sarun, R.P. Aloysius, U. Syamaprasad, Phys. C **433**, 28–36 (2005)
37. O. Bilgili, Y. Selamet, K. Kocabas, J. Supercond. Nov. Magn. **21**, 439–449 (2008)
38. M.A. Aksan, M.E. Yakinci, J. Alloys Compd. **385**, 33–43 (2004)
39. C. Terzioglu, M. Yilmazlar, O. Ozturk, E. Yanmaz, Phys. C 423, 119–126 (2005)
40. B. Ozkurt, J. Mater. Sci. Mater. **24**, 758 (2013)
41. B. Ozkurt, M.A. Madre, A. Sotelo, J.C. Diez, J. Mater. Sci. **24**, 1158 (2013)